CrystEngComm

ROYAL SOCIETY
OF **CHEMISTRY**

PAPER
Weikang Wang, Xiaoyan Cui, Ting Wang *et al.*
Twisted cholesterol crystals by Mueller matrix microscopy

Check for updates

Twisted cholesterol crystals by Mueller matrix microscopy†

Yue Tian,‡[a] Mengyuan Hao,‡[a] Yong Tang,[a] Chen Li,[a] Demei Kong,[a] Junru Zhu,[a] Weikang Wang, [ID] *[a] Xiaoyan Cui [ID] *[a] and Ting Wang [ID] *[bc]

Cholesterol crystals (CCs) are major contributors to atherosclerosis and gallstone development. Understanding the emergence, polymorphic variations, morphological intricacies, and molecular interactions of CCs are pivotal for unraveling associated maladies. We succeeded in growing CCs as spherulites in three polymorphs; two are banded spherulites composed of righthanded-twisted CCs. Moreover, all the CC spherulites can be stained by lipophilic dyes, such as Nile red and coumarin. The microstructures of twisted CCs in stained spherulites are explored in detail using the Mueller matrix microscope. Insights gleaned from the polymorphic diversity and microstructural characteristics of CCs offer valuable cues for elucidating their pathological cascades.

Introduction

Pathological crystallization of cholesterol *in vivo* is a complex process that has been discussed for a long period. Cholesterol, a crucial constituent of the plasma membrane, plays a pivotal role in regulating membrane properties and holds great physiological significance.[1,2] Cholesterol homeostasis is sophisticatedly balanced by the dynamics in the synthesis, uptake, and removal of cholesterol in living organisms. However, aberrant cholesterol accumulation in cells under pathological conditions may lead to cholesterol crystallization, contributing to various diseases such as hyperlipidaemia, gallstones,[3] and numerous cardiovascular diseases.[4–6] Notably, cholesterol crystals (CCs) serve as a fundamental driving force in atherosclerosis,[7,8] a classic cardiovascular disease. Many CCs are observed in advanced atherosclerotic plaque.[9,10] These rigid and sharp CCs are implicated in physically damaging fragile biostructures and eliciting a systemic inflammatory response that perpetuates the chronic development and progression of atherosclerosis.[11,12] Exploring the formation, growth, polymorphs, dynamics, and morphologies of CCs is essential for understanding, preventing, diagnosing, and treating diseases related to abnormal cholesterol metabolism.

As an amphipathic molecule featuring a rigid steroid ring and a hydrocarbon tail, the documented crystal structures of cholesterol consistently exhibit the characteristic bilayer arrangement observed in biological membranes:[13,14] the hydrophilic portion of the bilayer structures forms corrugated layers held together by hydrogen bonds, sometimes accompanied by water molecules.[15–17] Under physiological conditions, cholesterol typically crystallizes into triclinic monohydrate cholesterol[16] and triclinic anhydrous cholesterol.[17] Additionally, monoclinic cholesterol monohydrate[15] has also been observed. Scientists posit that the crystal structures of cholesterol retain a memory of their biological origins,[18] thus closely resembling precursor structures found in living systems. These various CC morphologies may exert distinct impacts on biological systems due to their different distributions and shapes. For instance, needle-like CCs tend to penetrate endothelial barriers and disrupt biostructures, leading to necrotic effects, vascular coagulation, and inflammatory diseases.[12] Plate-like CCs, on the other hand, are frequently observed in gallstone sections.[3] Furthermore, the morphology of cholesterol crystalline plaques is more than the ultimate manifestation of the crystals and the outcome of pathological processes. It encapsulates essential information about the biological environment related to the pathology. However, elucidating the pathological involvement of cholesterol in complex living organisms via crystallographic analysis is nontrivial.

The complex environment *in vivo* leads to the formation of single crystals and polycrystals of polymorphic CCs in atherosclerotic plaques. Cholesterol is also extensively

[a] School of Chemistry and Molecular Engineering, East China Normal University, 500 Dongchuan Road, Shanghai, 200241, China.
E-mail: wkwang@chem.ecnu.edu.cn, xycui@chem.ecnu.edu.cn
[b] Shanghai Skin Disease Hospital, School of Medicine, Tongji University, 1278 Baode Road, Shanghai, 200443, China. E-mail: wangting1983927@gmail.com
[c] Shanghai Engineering Research Center of Topical Chinese Medicine, 1278 Baode Road, Shanghai, 200443, China

† Electronic supplementary information (ESI) available. See DOI: https://doi.org/10.1039/d4ce01252f

‡ Both authors contributed equally to the work.

crystalized in radial concentric rings in many gallstone sections as spherulites,[3,19] although these cholesterol spherulites have been rarely studied. The limited exploration into cholesterol polycrystals further impedes understanding pathological cholesterol plaques. Therefore, delving into the growth and resulting superstructures of CC polycrystals is paramount for comprehending the mechanisms underlying cholesterol crystallization and the development of pathological crystals. Moreover, the specific interactions of external compounds with CCs have offered great potential for inhibiting CCs from molecular aspects. Dyes are unique additives for crystals, and the specific interaction between the dyes and the crystalline surface has orientated the dye molecules, resulting in orientated electric dipole moments.[20] As a result, the orientated absorption can be strong and straightforward indicators for the orientation of additives.[21,22] Extensive efforts are devoted to the dyed crystals for the molecular interaction of crystalline surface and additives.[23,24] Moreover, staining of cholesterols *in vivo* has attracted great attention, and CCs can be an efficient and simplified model for the staining of bilayer cholesterol in cellular membranes. Thus, we explored the potential staining of cholesterol in CCs.

Mueller matrix microscopy (MMM) is a non-destructive imaging technique with robust spatial resolution that captures extensively polarized information. By rotating a pair of quarter-wave plates with respect to two stationary crossed-linear polarizers, the time-averaged polarization states of light before and after passing through the sample can be obtained and subsequently demodulated to recover the full Mueller matrix (M). M presents as a 4 × 4 array of pseudo-colour images that can be transformed to another 4 × 4 matrix L. L is directly associated with polarization properties, including circular dichroism (CD), circular birefringence (CB), linear birefringence (LB), linear dichroism (LD), and the respective orientations of LB and LD. Rich information from the Mueller matrix analysis leads to great potential in the structural analysis of complex materials,[25,26] including living tissues,[27,28] chiral materials,[29,30] and polycrystalline structures such as banded spherulites, *etc.*[31–34]

Here, we synthesized three polymorphs of cholesterol spherulites *in vitro*, two of which were ring-banded spherulites. We used a polarization optical microscope, scanning electronic microscope, and Mueller matrix microscope to analyse the structure of spherulites. The two banded spherulites composed of twisted CCs are aggregations of right-handed twisted crystalline fibers. Banded CC spherulites are dyed with different lipidic dyes. Moreover, the microstructures of twisted CCs are detailedly explored with a Mueller matrix microscope. The full exploration of polarization states for the microstructural analysis by optical analysis was achieved by coumarin-dyed CCs banded spherulites. The evaluation of growth conditions and microenvironment-related polymorphs and microstructures of twisted CCs are informative for exploring their pathological processes and potential exploration of therapeutic medication.

Results and discussion

Crystal optics and morphologies

Three optically negative cholesterol spherulites are grown under distinct growth conditions (Fig. 1 and S1†). Grown from supercooling of the melt at different temperatures (T_m = 180 °C), two polymorphs of anhydrous cholesterol polycrystals are achieved: polymorph I (Fig. 1d) and polymorph II (Fig. 1e). Both polymorphs are optically double-banded, concentric ring-banded structures with alternating bright and dark rings under crossed polarizers. Monohydrate cholesterol crystallized as spherulites with relatively low linear retardance from its aqueous solution in poly(vinyl) alcohol (PVA) gel (Fig. 1f).

The PXRD and Raman spectra confirm the triclinic crystal structures of anhydrous cholesterol-banded spherulites (Fig. 2). Polymorph I crystallized in the space group of $P1$ with a = 10.2780(9) Å, b = 14.0688(12) Å, c = 33.990(3) Å, α = 96.047(2)°, β = 94.543(2)°, and γ = 90.441(2)°.[35] Polymorph II crystallized in the space group of $P1$ with a = 27.565(10) Å, b = 38.624(16) Å, c = 10.748(4) Å, α = 93.49(3)°, β = 90.90(3)°, and γ = 117.15(3)°.[36] The largest crystallographic plane of polymorph I is the (001) plane, and the banded spherulites grow along the crystallographic direction <100> (Fig. 2a). Moreover, the largest plane of polymorph II is the (010) plane, and the banded spherulites grow along <001> (Fig. 2b). The Raman results of the two polymorphs are in accordance with the typical Raman signals of cholesterol. The characteristic Raman scattering at 2850 cm^{-1}, 2866 cm^{-1}, 2903 cm^{-1}, 2932 cm^{-1} and 2959 cm^{-1} are all in the C–H
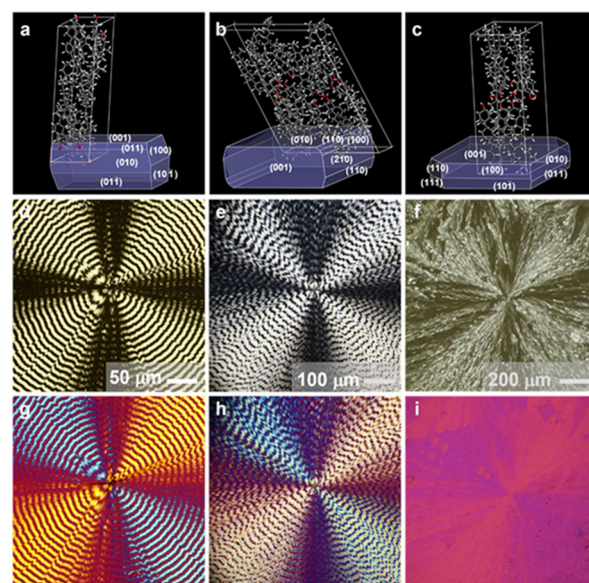
Fig. 1 Different polymorphs of cholesterol spherulites. Left column is banded anhydrous cholesterol spherulite polymorph I, the middle column represents polymorph II, and the right column is monohydrate cholesterol. (a–c) Bravais–Friedel–Donnay–Harker (BFDH) morphologies, (d–f) optical images of cholesterol spherulites under crossed-polarizers, and (g–i) with a 530 nm phase delay.
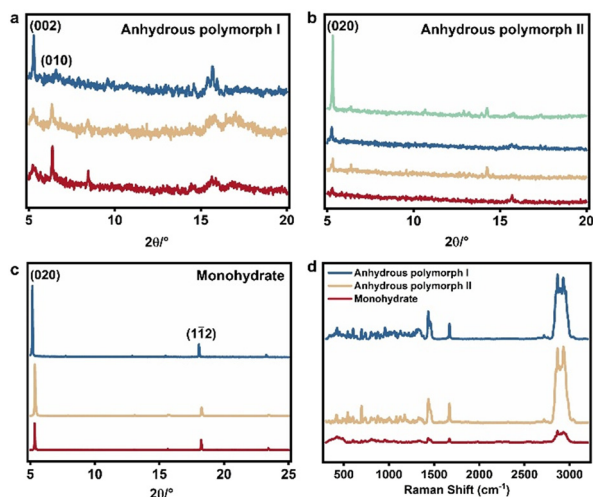
Fig. 2 Crystal structure of cholesterol spherulites. XRD pattern of (a) anhydrous cholesterol banded spherulite polymorph I, (b) anhydrous cholesterol banded spherulite polymorph II, (c) monohydrate cholesterol spherulites. Raman spectra (d) of three polymorphs of cholesterol spherulites.

stretching vibration region (2700–3100 cm^{-1}) of cholesterol molecules, and the peaks at 1433 cm^{-1} pertain to the methylene deformation zone (1400–1500 cm^{-1}), indicating that the composition of both the two banded-spherulites polymorphs is cholesterol (Fig. 2d).

Craven[16] found that the monohydrate cholesterol crystallizes in the space group of $P1$ with $a = 12.39(3)$ Å, $b = 12.41(3)$ Å, $c = 34.36(6)$ Å, $\alpha = 91.9(1)°$, $\beta = 98.1(1)°$, and $\gamma = 100.8(1)°$, and they also postulated that the unit cell of the monohydrate cholesterol single crystal adopted a layered structure, within which the hydroxyl and water molecules of cholesterol formed a two-dimensional hydrogen bond network on the ab plane, and the adipose ring was arranged parallel to the c-axis. We fabricated cholesterol monohydrate spherulites by adding drops to a thick PVA gel. The PXRD results are essentially consistent with the standard diffraction peak of cholesterol monohydrate. Thus, we contend that the spherulites growing in the PVA gel are composed of innumerable tiny cholesterol monohydrate single crystals, and the growth direction is <010> (Fig. 2c). Raman spectroscopic characterization also attested that the spherulites grown in the gel pertained to cholesterol (Fig. 2d).

At least around a quarter of organic molecules can form banded spherulites,[37,38] and periodic twisting of the composed crystalline fibrils is one of the most important reasons for the banded features.[39] Generally, the altered growth conditions, such as the existence of additives and the viscosity of the growth media, may impact their growth. These fibrils preserved the environmental information in specific situations as plastic deformation in twisting. Herein, the morphologies of CCs are evaluated in detail by SEM. Bundles of cholesterol crystalline lamellae around 3–10 μm in width and 100–200 nm in thickness aggregated radially to spherulites. It also can be

clearly observed that the side elevation (edge-on) and flat surface (flat-on) appear periodically. Superimposing the SEM and POM images suggested the exact periodicity of twisted morphologies and optical oscillation of lamellae. The edge-on and flat-on fall into the regions between bright and dark bands in both polymorphs. Compared with the relatively smooth surface in banded spherulites of polymorph I, the slightly rough and irregular surface in polymorph II indicates distinct mechanic properties in the two spherulites composed of twisted cholesterol fibrils (Fig. 3). Right handed-twisted lamellae oscillating between edge-on and flat-on are vividly preserved in the SEM images. In the banded spherulites of anhydrous cholesterol (polymorph I), tiny crystalline fibrils twisted along the <100> growth direction (Fig. S2†). In polymorph II, the bundles of lamellae twisted radially along <001> (Fig. S3†). For monohydrate cholesterol spherulites, crystalline fibrils with enormous recrystallization of tiny plates grow radially and form spherulites. The habits of crystalline plates in the spherulites indicate that the growth direction is <010> (Fig. S4†).

Mueller matrix analysis

We explored the microstructures of the banded cholesterol spherulites through optical analysis using a home-built Mueller matrix microscope (MMM). The design and principle are well explained in the literature.[31–34,40] In general, spherulites with a lower interference color have a smaller |LB|. CB originates from the helical overlapping of the crystalline cholesterol fibers. Thus, CB is the complex result related to the thickness of the spherical crystals, the number of fibers in a bundle, the |LB| of the fibers and the torsion angle of the fibers, which can reflect the chiral information of the spherulites. |LD| and CD reflect the absorption of banded-spherulites, and a significant enhancement of |LD| and CD signals is usually observed with the addition of
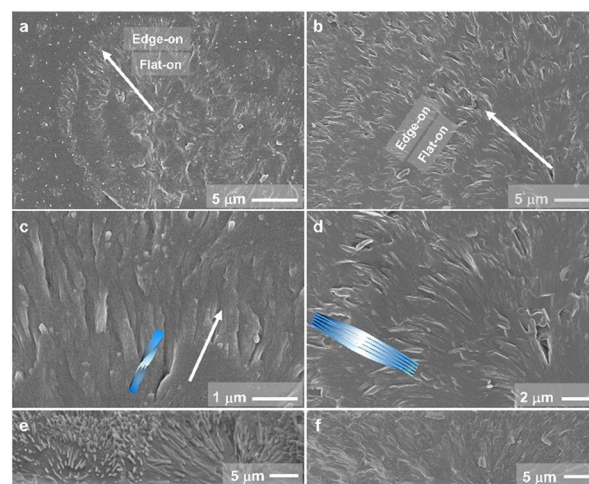
Fig. 3 SEM images of banded anhydrous cholesterol spherulites: (a, c and e) polymorph I and (b, d and f) polymorph II. The represented helical structures are superimposed in (c) and (d) as blue bundles. (e and f) Cross-sectional SEM images of the corresponding polymorphs.
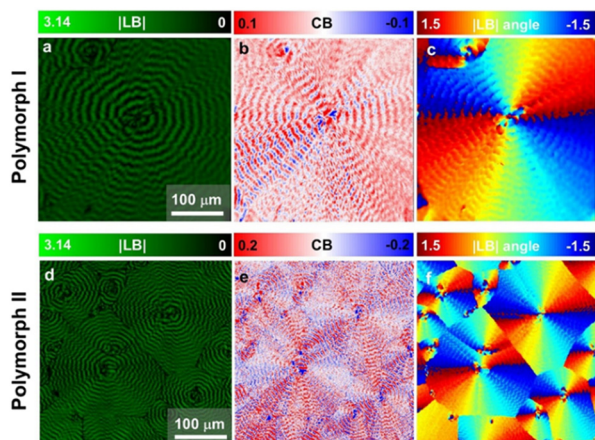
Fig. 4 MM results of banded cholesterol spherulites of polymorph I (a–c) and polymorph II (d–f) at 530 nm. (a and d) |LB| images, (b and e) CB images, and (c and f) LB angle images.

chromophores. As confirmed by the MMM imaging of both polymorphs, the intensity of |LB|, |LD|, CB, and CD oscillate along the spherulite radii. |LB| and |LD| are in phase, while CB and CD are out of phase. The same oscillating period but with ~π/4 phase shift is observed in the optical properties: max or min |LB| corresponds to zero CB, while CB with max intensity falls in the regions between max and zero |LB|. The similar optical features of both polymorphs are evaluated in detail (Fig. 4). For polymorph I, |LB| is approximately 0.28–1.25 rad, CB is approximately −0.12–0.24 rad, and the maximum value of CB occurs in the transition region from the maximum to the minimum of |LB|. For polymorph II, |LB| is approximately 0.4–1.25 rad, CB is approximately −0.05–0.15 rad, and the maximum value of CB occurs in the transition region from the minimum to the maximum value of |LB|.

We analyzed the optical properties through a Mueller matrix-based optical simulation for both polymorphs to explore the microstructure-resulted optical features. The detailed protocol and source codes are available in a previous publication.[32] In polymorph I, 20 layers of lamellae (for single lamella, the thickness is 170 nm and the width is 3.4 μm) composed a bundle of crystalline fiber. During the growth of banded spherulites, fibers twist along the growth direction, accompanied by the smooth oscillation of refractive indices, estimated as $[n_x, n_y, n_z]$ = [1.549, 1.536, 1.519]. The bundles of lamellae reached the maximum misalignment of 20° (thus, misalignment for adjacent lamellae is ~1.05°) between edge-on and flat-on regions (Fig. S5†). In polymorph II, 30 layers of lamellae (thickness ~110 nm, width ~3.3 μm) are bundled together to twist along the growth direction with $[n_x, n_y, n_z]$ = [1.581, 1.548, 1.564]. The maximum misalignment is around 25°, slightly larger than polymorph I, although the misalignment between adjacent lamellae is reduced to ~0.86° (Fig. S6†). Distinct misalignments with polymorphs suggest their specific mechanical properties, which agree with their different surface morphologies.

Monohydrate cholesterol spherulites have no banding and possess a very low birefringence. The orientated LB by MMM for monohydrate spherulites has also confirmed its crystalline structure (Fig. S7†). The MMM measurement outcomes of monohydrate cholesterol spherulites are in accordance with those of polarizing microscope images. Both |LB| and CB are extremely low, with |LB| approximately 0.15 rad and CB approximately −0.07 rad, and numerous stray signals exist.

Stained banded cholesterol spherulites

CCs are prone to include dyes in their crystalline structures. Many commercially available lipophilic dyes, such as Nile red, oil red O, and Sudan IV can be incorporated in the banded cholesterol spherulites during crystallization from the melt. The transition moments of the dye can be arranged explicitly in cholesterol fibers, producing varying degrees of absorption as the fibers spiral grow, which can be observed under fluorescence microscopy (Fig. S8†).

To acquire a more profound comprehension of the adsorption mechanism of dye molecules on the cholesterol crystal planes, we assessed the adsorption energy of dye molecules interacting with various crystal faces during crystal growth utilizing molecular simulation. Adsorption energy indicates the binding strength of dye molecules to a specific crystal surface, and the lower adsorption energy reflects the better adsorption effect. Herein, we analyzed the adsorption of coumarins on the (100) (010), (001), (1̄10), and (01̄1) planes of the anhydrous cholesterol crystal (polymorph II with #CCDC: 184885) by Materials Studio using Adsorption Locator and Forcite Modules (Fig. 5).[41] We evaluated the adsorption of dye molecules on five crystalline plates. The adsorption energies for coumarin are −18.6 kcal mol⁻¹ on (100), −19.6 kcal mol⁻¹ on (010), −21.7 kcal mol⁻¹ on (001), −20.4 kcal mol⁻¹ on (1̄10), and −15.3 kcal mol⁻¹ on (01̄1), respectively. The energetically preferred crystalline surface of
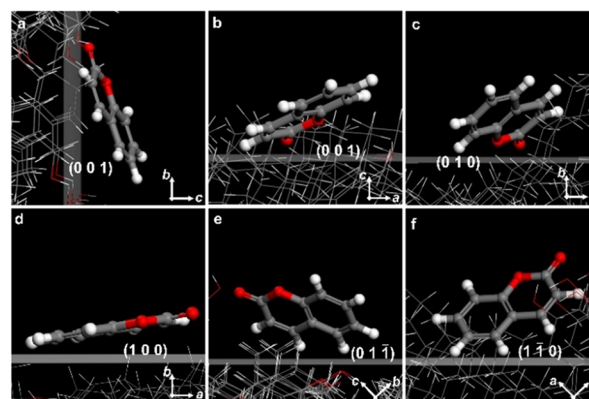

Fig. 5 Adsorption configurations of coumarin molecules on different crystal planes of anhydrous cholesterol crystal (polymorph II) in vacuum. (a) and (b) (001) viewed along the a- and b-axis, (c) (010), (d) (100), (e) (01̄1), and (f) (1̄10).

coumarin is (001), where the conjugated π-systems of coumarin molecules are inclined to the (001) plane with the electronic dipole moment nearly parallel to the b-axis.

We also succeeded in dyeing CCs with coumarin. The strong interaction between dyes and helicoidal crystals is demonstrated by the oscillated anisotropy of the dye adsorption as a result of the twisted transition electric dipoles of the dye process around the twisting axes of each helicoid (Fig. 6a–c). Moreover, all the evaluated lipophilic dyes are aligned orthogonal to the growth direction of the helicoidal CCs, eliminating the possibility of passive inclusion during growth. For the well-aligned dyes in banded spherulites, as confirmed by the micrograph with a linear polarizer, the transition moments of the dyes are normal to the radii. Albeit the tangential alignment is much rarer than the radial arrangement in dyeing spherulites,[42] the simulated micrograph for the tangential alignments of dyes agreed well with the experimental observation for the three evaluated chromophores (Fig. 6d). As we observed in the SEM, polarized microscopy, and simulation results, the polymorph II twisted radially along <001>, while coumarins are normal to the growth direction, resulting in oscillated LD along the

radii growth direction of spherulites. Similar alignments are observed in both polymorphs.

Thus, we have confirmed that cholesterol crystals are uniquely adaptable crystalline hosts for lipophilic guests through strong interaction. Staining cholesterol crystals can be a straightforward approach to exploring the interaction of lipophilic molecules and cholesterol, which is crucial in the potential analysis of transmembrane molecules in biosystems. Thus, the lipophilic guests may prefer to dock on the (001) plane, potentially impacting the growth of CCs. These findings may offer some hints for the therapy of CCs-related diseases from the aspect of crystallography.

The aligned dyes also profoundly impacted the optical properties of cholesterol-banded spherulites. Due to the vertical alignment of dyes in terms of the growth direction of spherulites, |LD| and CD are oscillated, although the scattering effects are omitted in the simulation. Banding structures of the stained banded cholesterol spherulites are observed in all the optical properties (Fig. 6e–h). The LD angle in MMM results have confirmed the tangentially aligned transition electric dipole moments (Fig. 6k). Moreover, the complete optical properties of dyed spherulites
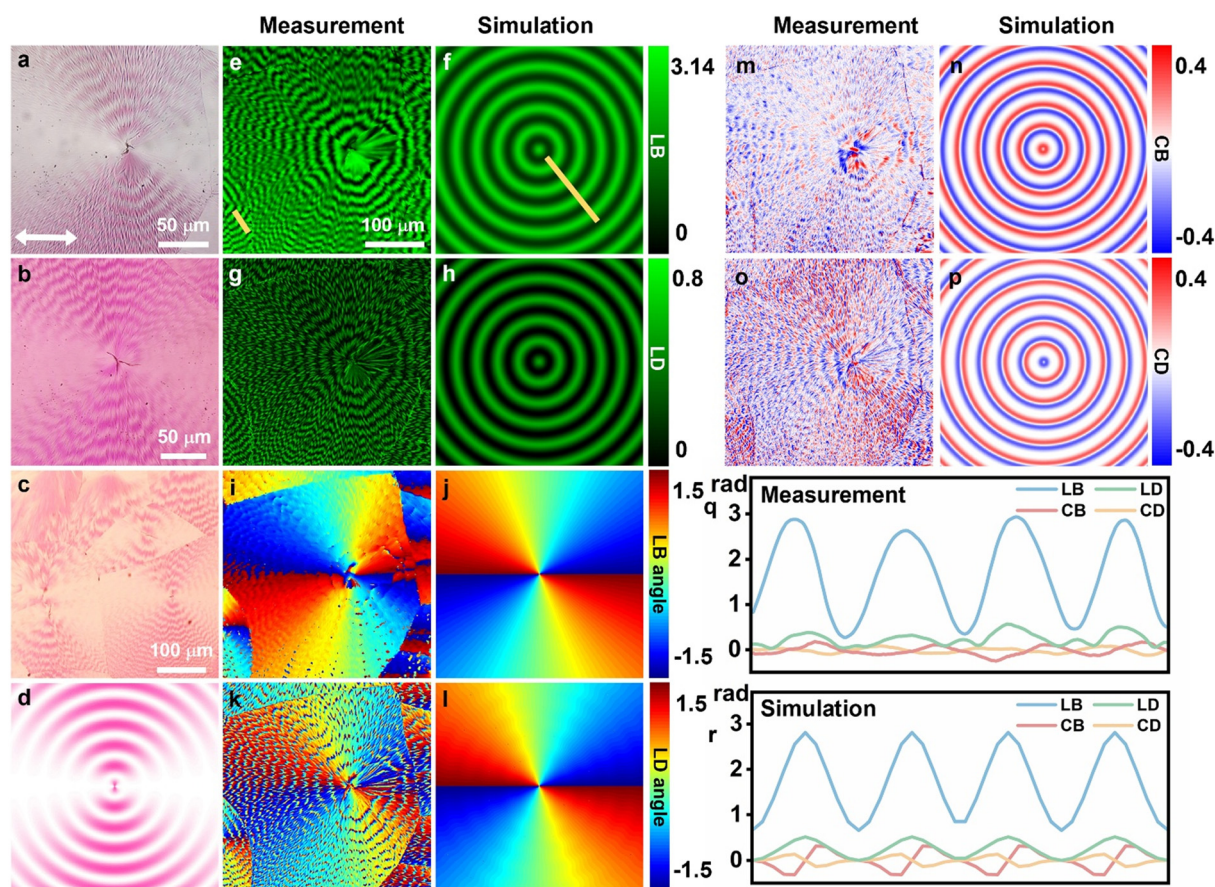
Fig. 6 Micrographs of stained banded anhydrous cholesterol spherulites (polymorph II). 0.5 wt% (a) Nile red, (b) oil red O, (c) coumarin dyed-cholesterol spherulites, and (d) the simulated transmission images with dyes arranged perpendicular to the radii. Experimental (left) and simulated (right) optical results of dyed spherulites at 550 nm: (e and f) |LB|, (i and j) |LD|, (g and h) CB, (k and l) CD, (m and n) LB angle, and (o and p) LD angle. (q) Experimental and (r) simulation results of the optical properties extracted along the yellow lines in (e) and (f).

were simulated by introducing the total permittivity of the dye as a complex B in the Mueller matrix-based optical analysis.[32] In short, B is a complex-valued amplitude for an oscillator that depends on the wavelength, affecting total permittivity and generating specific differential Mueller matrix parameters. The real part of B is the contribution to dispersion, and its imaginary part is related to the absorption. $B = -0.035 - 0.025i$ in polymorph I, and $B = -0.12 - 0.04i$ in polymorph II, as confirmed by the LD and CD results in simulation (Fig. 6g, h, o and p). In the simulated CD for both polymorphs, the oscillation periods and intensities of all the optical properties agreed well with the experimental observation (Fig. 6q and r). The results are shown in the ESI† (Fig. S9). Thus, we have unveiled the microstructures of cholesterol-banded spherulites with comprehensive optical analysis. Moreover, the alignment of dyes in cholesterol crystals has been confirmed in the optical features of the polycrystalline structures, offering extensive potential in their application *in vivo*.

Conclusions

We have explored the aggregation of infinite right-handed twisted crystals, leading to the formation of polycrystalline structures, such as the ring-band spherulites. It has also been demonstrated that the two polymorphs of cholesterol banded spherulites are constituted by right-handed twisted cholesterol fibers, yet possess distinct mechanical properties. The spherulite of cholesterol monohydrate exhibits a central divergence, and the spherulite nucleus is analogous to that of the cholesterol monohydrate plate single crystal. Through the systematic application of Mueller matrix microscopy, we analyse and scrutinize the microstructural variances inherent in different crystalline structures, providing essential methodologies and insights for future research endeavours.

Data availability

The data supporting this article have been included as part of the ESI.†

Author contributions

Y. Tian and M. H.: crystal growing, crystal investigation, writing, editing; Y. Tang, C. L., D. K., and J. Z.: crystal analysis; T. W., X. C., and W. W.: funding acquisition, writing, review, and editing. All authors have read and agreed to the manuscript.

Conflicts of interest

There are no conflicts to declare.

Acknowledgements

Notes and references

1 M. Zhang, L. Li, D. Fang, T. J. Kelley and J. D. Burgess, *Anal. Chem.*, 2018, **90**, 5903–5908.

2 A. G. Ayuyan and F. S. Cohen, *Biophys. J.*, 2018, **114**, 904–918.

3 E. I. Suvorova, V. V. Pantushev and A. E. Voloshin, *Crystallogr. Rep.*, 2017, **62**, 817–830.

4 A. Grebe and E. Latz, *Rheumatol. Rep.*, 2013, **15**, 313.

5 T. Speer, S. Dimmeler, S. J. Schunk, D. Fliser and P. M. Ridker, *Nat. Rev. Nephrol.*, 2022, **18**, 762–778.

6 O. Leavy, *Nat. Rev. Drug Discovery*, 2016, **15**, 309–309.

7 Y. Baumer, S. McCurdy, X. Jin, T. M. Weatherby, A. K. Dey, N. N. Mehta, J. K. Yap, H. S. Kruth and W. A. Boisvert, *Atherosclerosis*, 2019, **287**, 100–111.

8 B. Ho-Tin-Noe, S. Vo, R. Bayles, S. Ferriere, H. Ladjal, S. Toumi, C. Deschildre, V. Ollivier and J. B. Michel, *J. Pathol.*, 2017, **241**, 671–682.

9 G. T. Stewart, *Nature*, 1959, **183**, 873–875.

10 D. M. Small and G. G. Shipley, *Science*, 1974, **185**, 222–229.

11 N. Varsano, J. Capua-Shenkar, L. Leiserowitz and L. Addadi, *Annu. Rev. Mater. Sci.*, 2022, **52**, 57–78.

12 M. B. Al-Handawi, P. Commins, D. P. Karothu, G. Raj, L. Li and P. Naumov, *Chem. – Eur. J.*, 2018, **24**, 11493–11497.

13 R. Ziblat, K. Kjaer, L. Leiserowitz and L. Addadi, *Angew. Chem., Int. Ed.*, 2009, **48**, 8958–8961.

14 M. Shepelenko, A. Hirsch, N. Varsano, F. Beghi, L. Addadi, L. Kronik and L. Leiserowitz, *J. Am. Chem. Soc.*, 2022, **144**, 5304–5314.

15 I. Solomonov, M. J. Weygand, K. Kjaer, H. Rapaport and L. Leiserowitz, *Biophys. J.*, 2005, **88**, 1809–1817.

16 M. C. Bryan, *Nature*, 1976, **260**, 727–729.

17 H. S. Shieh, L. G. Hoard and C. E. Nordman, *Nature*, 1977, **267**, 287–289.

18 N. Varsano, F. Beghi, N. Elad, E. Pereiro, T. Dadosh, I. Pinkas, A. J. Perez-Berna, X. Jin, H. S. Kruth, L. Leiserowitz and L. Addadi, *Proc. Natl. Acad. Sci. U. S. A.*, 2018, **115**, 7662–7669.

19 K. Jayasoma, N. H. Koralegedara, A. Dharmapala and R. Chandrajith, *Biol. Trace Elem. Res.*, 2022, **200**, 4891–4902.

20 B. Kahr and R. W. Gurney, *Chem. Rev.*, 2001, **101**, 893–951.

21 B. Kahr and L. Vasquez, *CrystEngComm*, 2002, **4**, 514–516.

22 J. B. Benedict, J. H. Freudenthal, E. Hollis and B. Kahr, *J. Am. Chem. Soc.*, 2008, **130**, 10714–10719.

23 V. M. Hall, K. A. Cox, R. E. Sours and J. A. Swift, *Chem. Mater.*, 2016, **28**, 3862–3869.

24 N. Xue, M. Hao, Y. Tian, Y. Zhou, H. Chen, T. Wang, X. Cui and Y. Tian, *Cryst. Growth Des.*, 2024, **24**, 10073–10081.

25 X. Feng, B. Chen, D. Kong, T. Wang, X. Cui and Y. Tian, *J. Phys. Chem. C*, 2023, **127**, 6974–6980.

26 S. Bhunia, S. Chandel, S. K. Karan, S. Dey, A. Tiwari, S. Das, N. Kumar, R. Chowdhury, S. Mondal, I. Ghosh, A. Mondal, B. B. Khatua, N. Ghosh and C. M. Reddy, *Science*, 2021, **373**, 321–327.

27 I. Pardo, S. Bian, J. Gomis-Brescó, E. Pascual, A. Canillas, S. Bosch and O. Arteaga, *J. Biophotonics*, 2024, **17**, e202300252.

28 T. Liu, M. Lu, B. Chen, Q. Zhong, J. Li, H. He, H. Mao and H. Ma, *J. Biophotonics*, 2019, **12**, e201900151.

29 T. Duan, J. Ai, X. Cui, X. Feng, Y. Duan, L. Han, J. Jiang and S. Che, *Chem*, 2021, **7**, 2695–2707.

30 H.-M. Ye, J. H. Freudenthal, M. Tan, J. Yang and B. Kahr, *Macromolecules*, 2019, **52**, 8514–8520.

31 X. Cui, A. L. Rohl, A. G. Shtukenberg and B. Kahr, *J. Am. Chem. Soc.*, 2013, **135**, 3395–3398.

32 X. Cui, S. M. Nichols, O. Arteaga, J. Freudenthal, F. Paula, A. G. Shtukenberg and B. Kahr, *J. Am. Chem. Soc.*, 2016, **138**, 12211–12218.

33 X. Cui, A. G. Shtukenberg, J. Freudenthal, S. Nichols and B. Kahr, *J. Am. Chem. Soc.*, 2014, **136**, 5481–5490.

34 A. G. Shtukenberg, X. Cui, J. Freudenthal, E. Gunn, E. Camp and B. Kahr, *J. Am. Chem. Soc.*, 2012, **134**, 6354–6364.

35 A. R. Tyler, R. Ragbirsingh, C. J. McMonagle, P. G. Waddell, S. E. Heaps, J. W. Steed, P. Thaw, M. J. Hall and M. R. Probert, *Chem*, 2020, **6**, 1755–1765.

36 L. Y. Hsu, J. W. Kampf and C. E. Nordman, *Acta Crystallogr., Sect. B*, 2002, **58**, 260–264.

37 A. G. Shtukenberg, Y. O. Punin, E. Gunn and B. Kahr, *Chem. Rev.*, 2011, **112**, 1805–1838.

38 Y. Zhou, X. Feng, T. Wang, Y. Tian and X. Cui, *CrystEngComm*, 2021, **23**, 1439–1446.

39 A. G. Shtukenberg, E. Gunn, M. Gazzano, J. Freudenthal, E. Camp, R. Sours, E. Rosseeva and B. Kahr, *ChemPhysChem*, 2011, **12**, 1558–1571.

40 D. Gottlieb and O. Arteaga, *Opt. Express*, 2021, **29**, 34723–34734.

41 L. N. Poloni, Z. Zhu, N. Garcia-Vázquez, A. C. Yu, D. M. Connors, L. Hu, A. Sahota, M. D. Ward and A. G. Shtukenberg, *Cryst. Growth Des.*, 2017, **17**, 2767–2781.

42 J. B. Benedict, J. H. Freudenthal, E. Hollis and B. Kahr, *J. Am. Chem. Soc.*, 2008, **130**, 10714–10719.